Supplementary Figure 1: Snapshots of monolayer bacterial swarms with different aspect ratios (α) and densities (ρ). The qualitative differences between the swarming (S), small clusters (SC) and large clusters (LC) phases can be observed. The figure is similar to Fig. 1a in the main text, but for a much larger field of view.

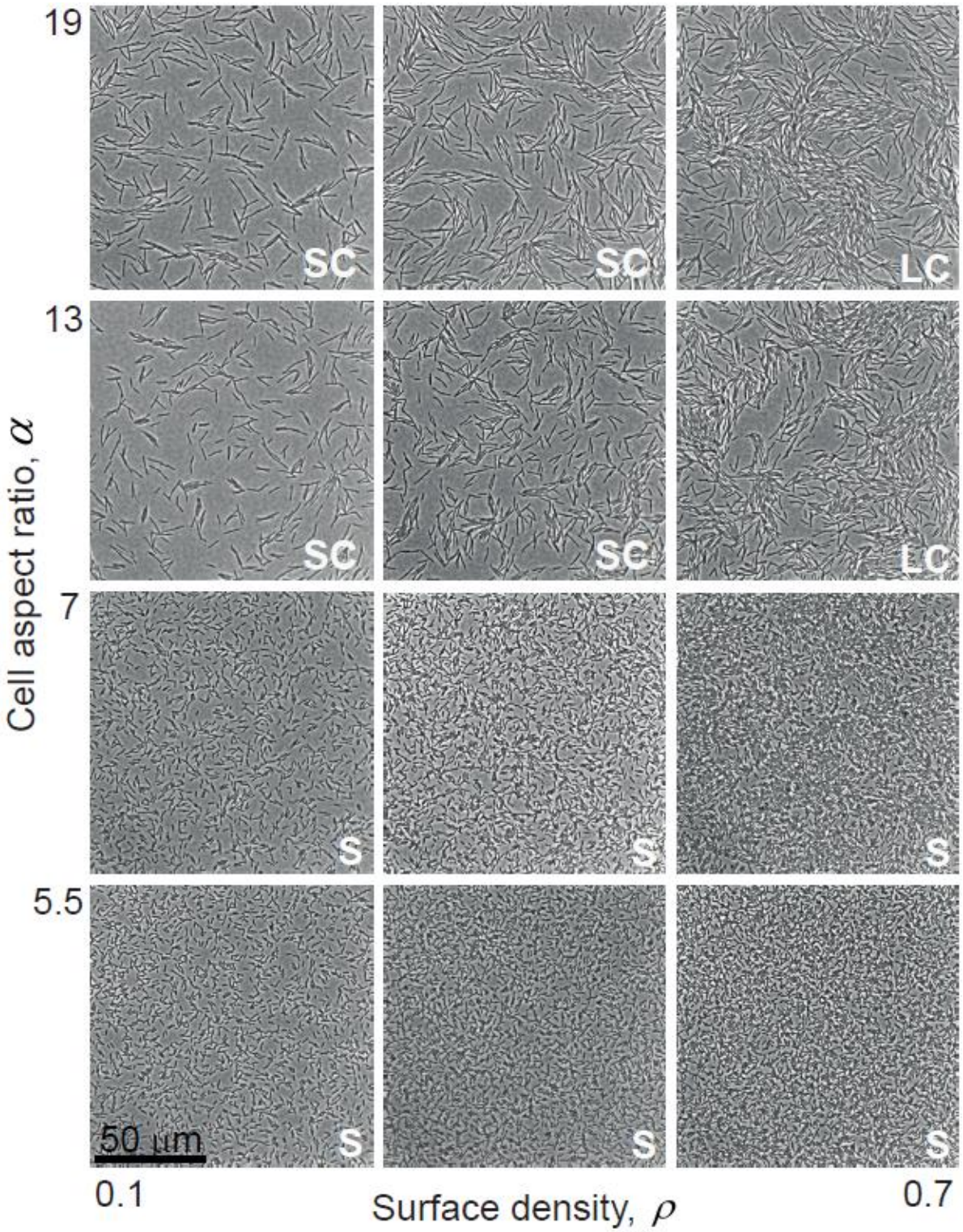

Supplementary Figure 2: Motility control experiments. Dots represent average values for each aspect ratio, error bars are the standard deviation. The black full line is the best linear fit as reported in each figure. **a**, The swimming ability of the bacteria in sparse (10^4 cells/ml) liquid suspensions. Both wild-type and mutants swam in the well-known 'run-and-tumble' mode with approximately similar speeds (~33 μm/s) during 'runs'. **b**, The ability of all strains to colonize LB (Luria-Bertani)plates is fairly constant. **c**, The standard deviation of cell aspect ratio as a function of mean cell aspect ratio. This indicates that relatively small, or large, deviations in cell length within a strain are not affecting the collective dynamics. **d**, Drops of overnight cultures were deposited on flat smooth plastic surfaces. The contact angles were nearly identical for all strains, indicating that the amount of surfactants secreted by cells is the same. **e**, Growth curves for the five strains (See supplementary Table 1 for the color code). The dashed line shows the lag time between the inoculation and expansion times, the dot-dashed line is a guide to the eye with a constant slope of 0.34, indicating the best-fit growth rate. **f**. Doubling time in liquid. Overall, these results indicated that all mutants have similar swimming and swarming capabilities with no apparent or immediate motility defects.

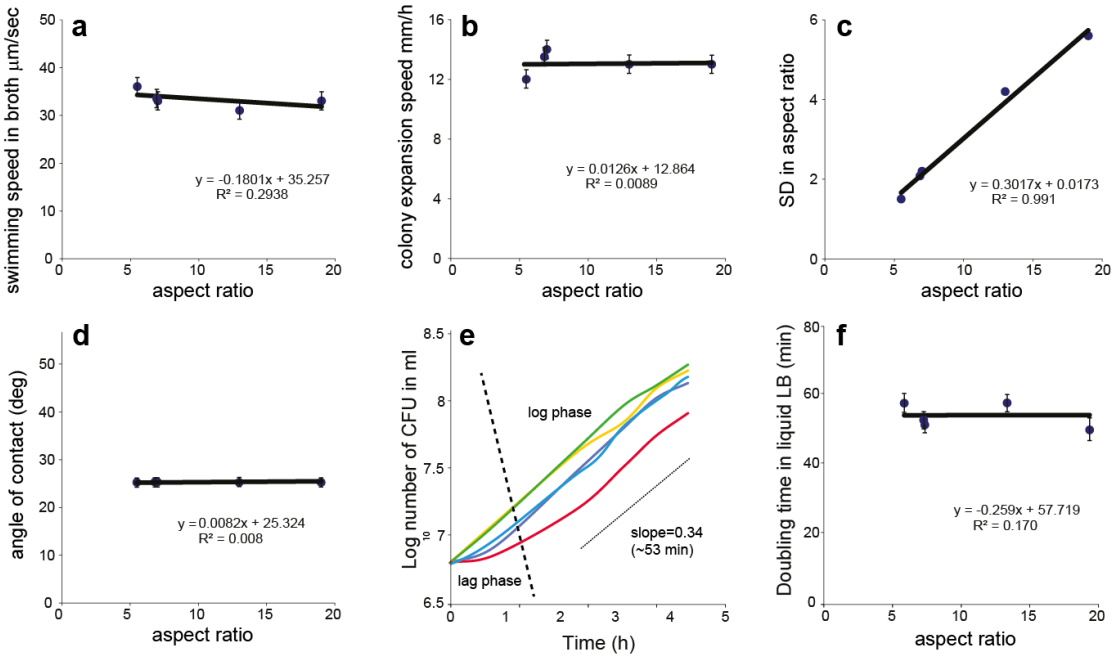

Supplementary Figure 3: Aspect ratio control experiment. The mutant strain DS860 (hollow circles) has an aspect ratio that is very similar to the wild type (blue squares). Accordingly, their swarming statistics for the (**a**) average speed, (**b**) temporal fluctuations and (**c**) Hurst exponent behavior as a function of the surface density are indistinguishable. The Square grey area represents the transition region between the small clusters (SC) and large clusters (LC) phases. Error bars represent the standard deviation and are of the same size as the marker.

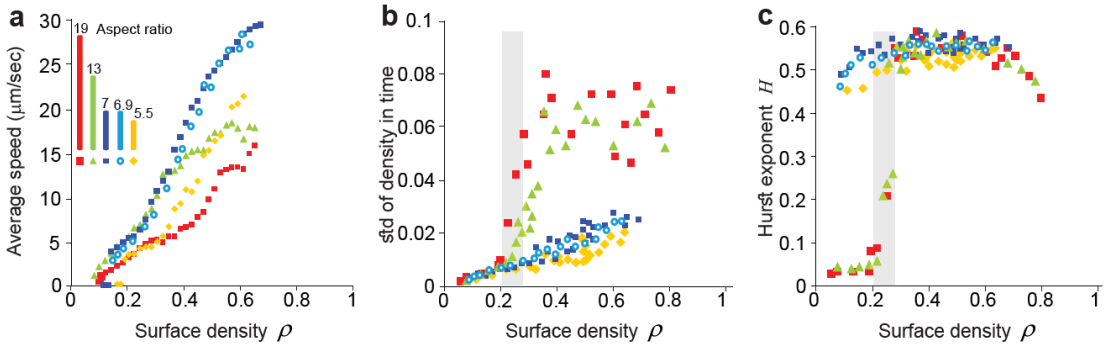

Supplementary Figure 4: Measurement of the spatial distribution. a, In order to estimate the spatial distribution of cells, all frames corresponding to a given density were partitioned into 10×10 bins (for illustration purposes, we only show a part of the full viewing field). **b**, The standard deviation among bins as a function of density and at different aspect ratios.

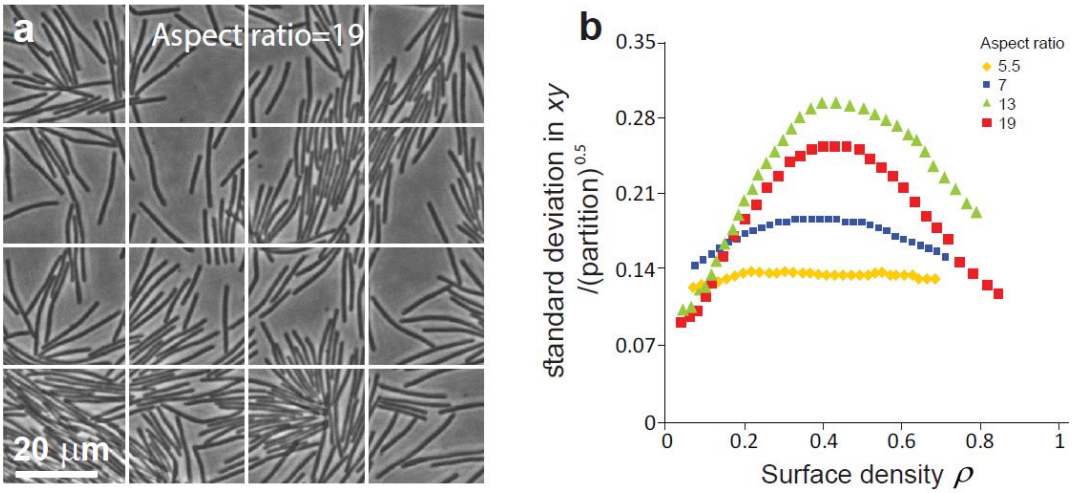

Supplementary Figure 5: Distribution of velocities. At small densities, the kurtosis (4^{th} moment) of the velocity distribution is much larger for large aspect ratios. Error bars represent the standard deviation (in the kurtosis) and are of the same size as the marker.

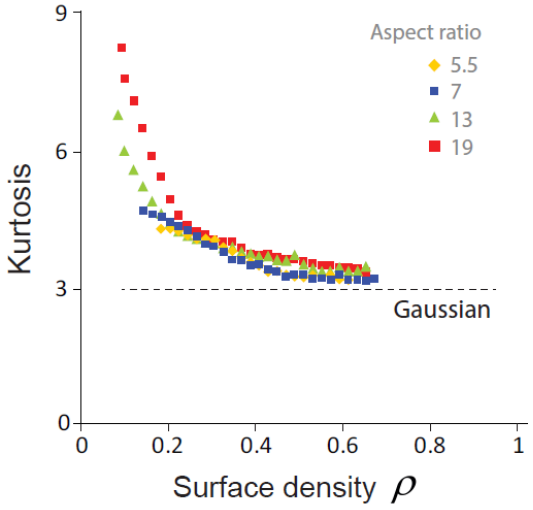

Supplementary Figure 6: Measurement of the temporal fluctuations. a, The Hurst exponent may be obtained for any time series or landscape, in this case for the instantaneous density, by taking the mean standard deviation <std> around the mean value (dashed horizontal line) for different "windows" of size Δt. **b,** If the time series (the landscape) is self-similar one will obtain a scaling of $<std> \sim \Delta t^H$ with H being the Hurst exponent. H Indicates the roughness of the landscape; with H~0.5 for a regular random walk H~0 for bounded fluctuations. **c,** Nine additional measurements, to the data shown in Fig. 4e, were performed, in order to study the influence of the field of view on the fluctuations. Three of the seven are cropped windows of the original data-set taken by the lens of 40×, reaching a very small window size; Three of them were taken by a smaller lens of 10× (one is cropped to the same size of the 40×); and three others were taken by a much smaller lens of 5× to achieve a very large field of view. See Supplementary Note 2 for a discussion of these results.

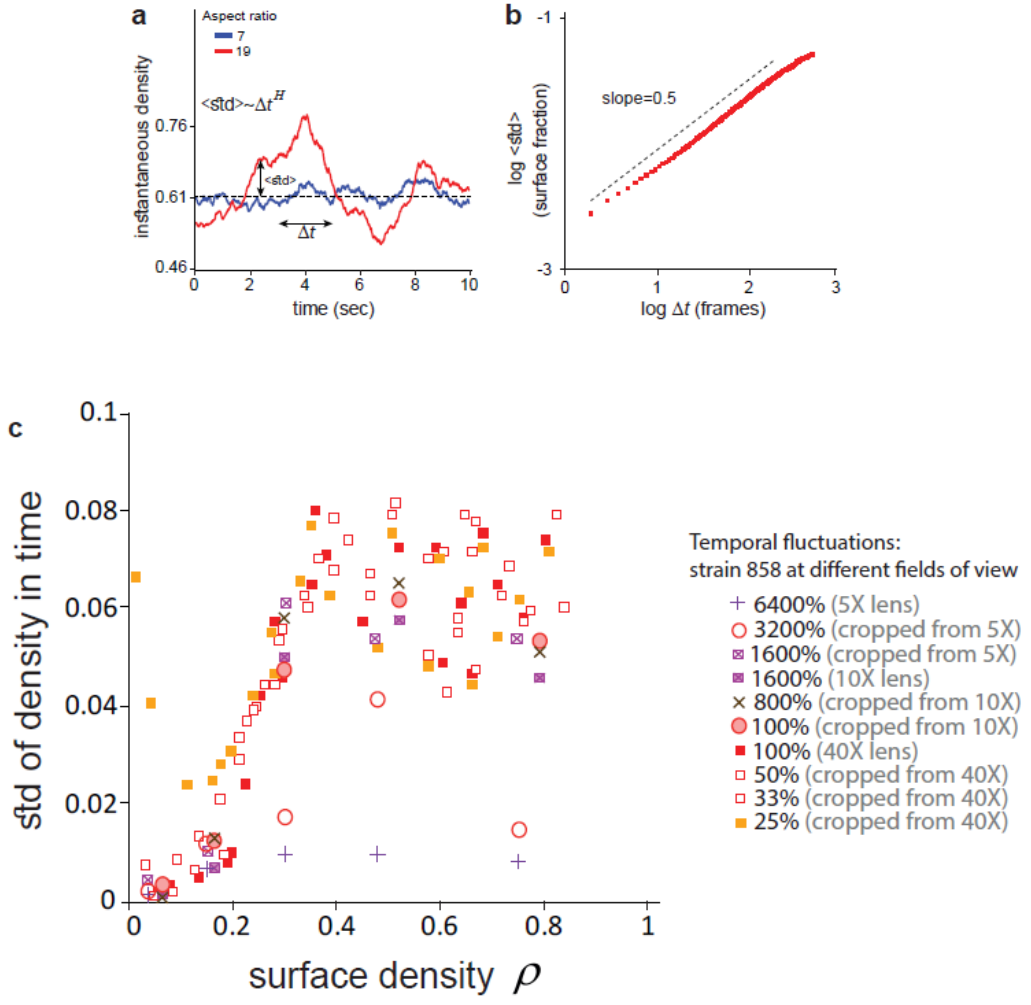

Supplementary Figure 7: Giant number fluctuations. a, The variance in the density among sub-regions as a function of average density and at different aspect ratios. See the methods section for details. While giant number fluctuations are observed, the effect is not as pronounced as predicted by theory and simulations. Each point corresponds to the slope of a log-log plot showing the standard deviation in sub-domains as a function of the average number of cells (relative to maximal concentration). **b,** four example plots corresponding to the four empty points in a.

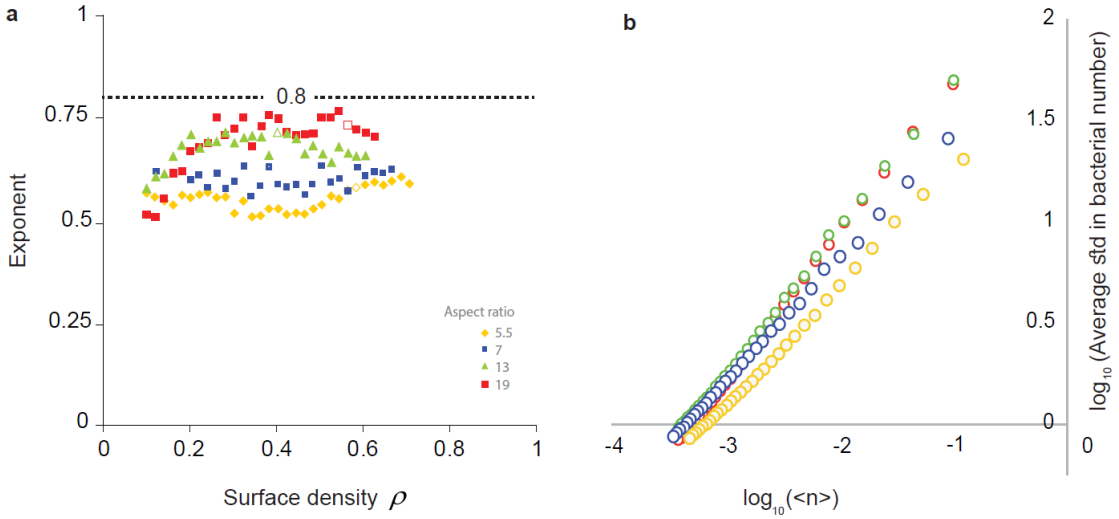

Supplementary Figure 8: Auto-correlation functions – velocity direction. The temporal auto-correlation function in the velocity direction decays (approximately) exponentially at all densities and aspect ratios. The figure depicts four examples plotted in both log-log (**a**, c **e**, **g**) and semi-log (**b**, **d**, **f**, **h**) scale. **a**-**b**, aspect ratio=5.5, density=0.52, **c**-**d**, aspect ratio=7, density=0.52, **e**-**f**, aspect ratio=13, density=0.52, **g**-**h**, aspect ratio=19, density=0.52. The characteristic time scale of short cells (swarm S phase) is about twice as small compared to long cells (small/large clusters phases). The auto-correlation in the velocity behaves similarly. Error bars represent the standard deviation and are of the same size as the marker.

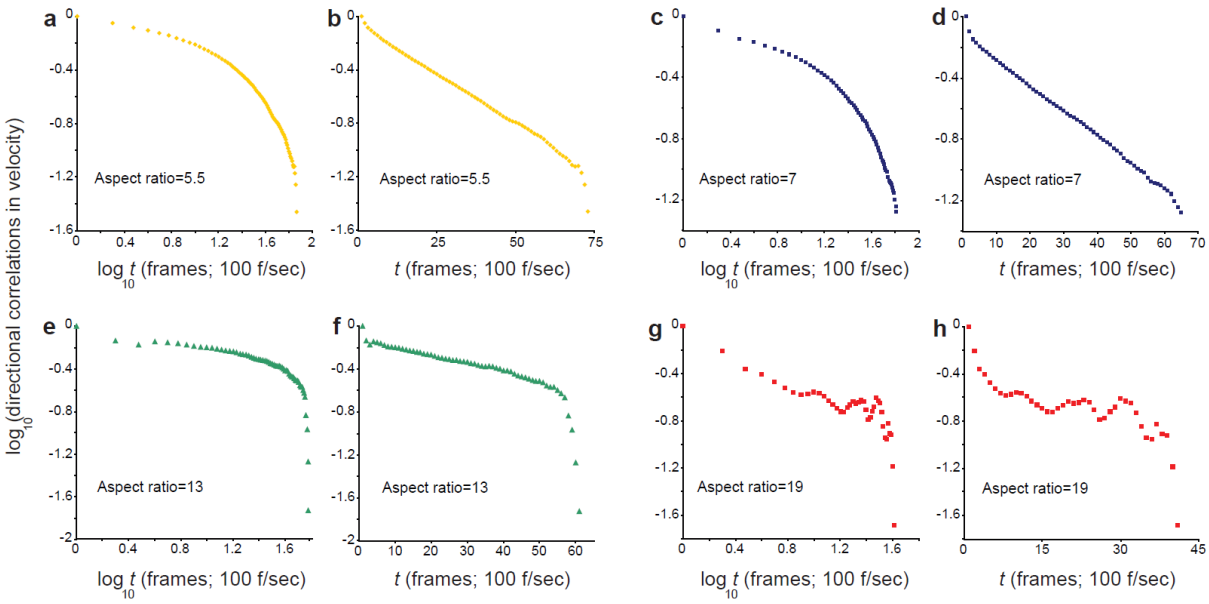

Supplementary Figure 9: Auto-correlation functions – cell orientation. The temporal auto-correlation function in the cell orientation. The figure depicts four examples plotted in both log-log (**a**, **c**, **e**, **g**) and semi-log (**b**, **d**, **f**, **h**) scale. **a**-**b**, aspect ratio=5.5, density=0.52, **c**-**d**, aspect ratio=7, density=0.52, **e**-**f**, aspect ratio=13, density=0.52, **g**-**h**, aspect ratio=19, density=0.52. The auto-correlation function of short cells (swarm S phase) shows two regimes – at short times the decay is exponential. At long times the decay seems to resemble a power-law. However, our statistics is not sufficient to determine this with accuracy. The auto-correlation function of long cells (small/large clusters phases) seems only exponential, although it is possible that the power-law behavior occurs at longer times, for which we have insufficient statistics. The characteristic time scale of short cells is about 2-3 times smaller compared to long cells. Error bars represent the standard deviation and are of the same size as the marker.

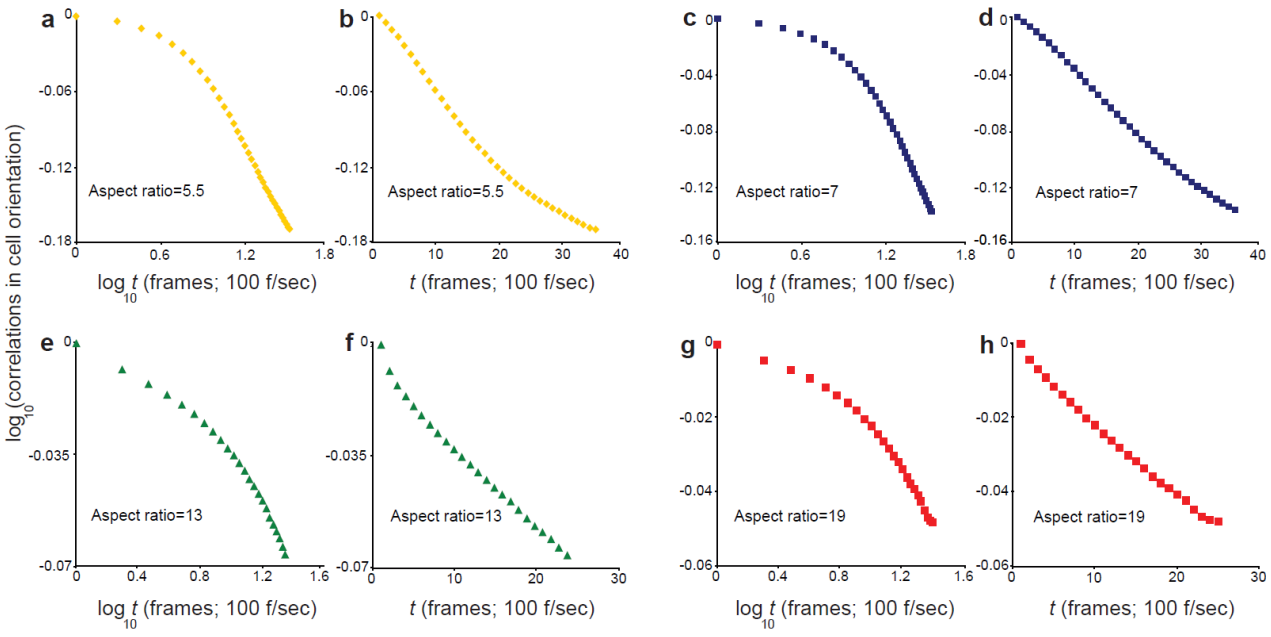

Supplementary Table 1: Strains data - Table. A summary of the *B. subtilis* 3610 strains used in this work. The mutation column describes the nature of the mutation used to generate the strain using the standard nomenclature for describing mutations and other sequence variations.

The *Bacillus subtilis* 3610 strains

Strain	Aspect ratio in swarm	Mutation
DS1470	5.5±1.5	swrA::tet amyE::Physpank-swrA spec
DS860	6.9±1.2	amyE::Physpank-swrA spec
WT	7.0±2.2	-
DS3774	13.0±4.2	minD::TnYLB kan
DS858	19.0±5.6	minJ::tet

Supplementary Note 1. Control experiments

In order to verify that the differences in the swarming dynamics statistics are only due to aspect ratio, several control tests were performed. This is important because the 3 strains (Supplementary Table 1) were generated in different ways, genetically affecting specific genes to form short or long cells.

- Supplementary Figure 2a shows that the swimming ability of the bacteria in sparse (10^4 cells/ml) liquid suspensions, where interactions between cells are negligible and there is no interaction with a surface, is the same for all strains. Both wild-type and the mutants swam in the well-known 'run-and-tumble' mode with approximately similar speeds (~33 μm/s) during 'runs' (mind that the cells in this experiment do not grow to the same aspect ratio as in the swarm experiment).
- Supplementary Figure 2b shows that the ability of all strains to colonize (Luria-Bertani) LB plates is fairly constant. All strains showed a macroscopic swarm pattern and covered a standard Petri-dish (8.8 cm) within a few hours, moving the colony front at approximately the same speed (~13 mm/h).
- Supplementary Figure 2c shows a linear trend in the standard deviation of cell aspect ratio for each strain as a function of mean cell aspect ratio. This indicates that relatively small, or large, deviations in cell length within a strain are not affecting the collective dynamics.
- In Supplementary Figure 2d, drops of overnight cultures were deposited on flat smooth plastic surfaces (10 μl on the inner part of the tap of a Petri-dish). The contact angles indicate the levels of surfactants secreted by the cells. This angle (~25°) was nearly identical for all strains (note that the surfactant experiments were performed on bacteria taken from swimming cells where swarming motility is not expressed; the cells in this experiment do not grow to the same aspect ratio as in the swarm experiment).
- Supplementary Figures 2e-f show growth curves for the four strains. Each strain was grown overnight from a plate stock (with the appropriate antibiotics) in a separate 50 ml tube in fresh LB broth (with no antibiotics) at 30ºC and shaking (200 RPM) (10 ml in each tube). The overnight cultures were diluted (1/100 fold) and regrown at same conditions. The number of colony forming units

(CFU) grown on 1.5% agar LB plates from these suspensions (after appropriate culture dilution) for each strain was counted; this was repeated during few hours from first dilution. The experiments were done few times so that the optical density was adjusted in all strains to yield same number of CFU in the starting culture. A summary of these measurements shows that the doubling time is similar in all strains (approximately 53 min) with very small variations in the duration of the lag phase. Overall, these results indicated that all mutants have similar swimming and swarming capabilities with no apparent or immediate motility defects.

Overall, these tests guaranty that on the single cell level, cell motility was not affected.

In addition, we have used another strain (DS860) that was defective similarly to the DS1470 (the only difference is that DS1470 has been deleted for the native copy of swrA). However, the aspect ratio of this strain remained similar to the wild-type. Our main results with this strain, namely the average microscopic speed, the density fluctuations in time, and the Hurst exponent, were found to be similar to those obtained for the wild-type, indicating that the mutation (at least in this specific strain) does not cause detectable changes in the dynamics. See Supplementary Figure 3 for more details.

Supplementary Note 2. Effect of field of view size on density fluctuations

In order to understand the effect of the finite window size on the fluctuations in density, the experiments were repeated using smaller magnifications, allowing a larger field of view. Note that individual cell tracking is not possible at these magnifications, but the density can be evaluated using the grey-scale images. Supplementary Figure 6c shows results for the longest mutant (DS858), where the fluctuations are more significant. At very large fields of view, 1.2×1.2 mm, 3200% of the original area, the temporal fluctuations are reduced. Following the interpretation of temporal fluctuations as large, dense clusters entering and leaving the field of view, this result suggests that clusters have a finite size, with maximal-sized clusters containing ~2000 cells.

Supplementary Note 3. Swarming bacteria and self-propelled rods

A popular model to account for the basic physics of interacting self-propelled agents such as swarming bacteria is the self-propelled rods (SPR) with steric interactions [1-7]. The experiments presented here do have features predicted in simulations of self-propelled rods, such as the transition from an exponentially decay cluster size distribution (CSD) in the swarming phase to a clustering phase with a bimodal CSD as shown in Fig. 3. Such a behavior has already been reported for a mutant myxobacterial species [8]. The transition to glassy or jammed dynamics at large densities is also a feature often captured by SPR models, see e.g. [3-4]. For the simulations of SPR with steric repulsion cited above, the product of the aspect ratio and density has often turned out to be a crucial control parameter for the onset of collectivity as well as for the emergence of spatial patterns such as polar cluster reflecting a basic property of Onsager`s famous theory for the isotropic-nematic phase transition in colloidal rods [9]. This property is in contrast to the observation presented here that the transition from the swarming phase to the clustering phases is only weakly dependent on the density and shifted also to larger aspect ratios in comparison to SPR simulation.

In addition, the bacteria studied here also require proximity to sufficiently many other bacteria in order to move on the agar surface, whereas individual SPR move at a prescribed typical speed independent of the local bacterial density. This strong nonlinear dependence of the velocity on the density should also be incorporated in a future model in order to achieve a quantitative description of the experiments in this work. A direct inspection of the snapshot in the clustering phase shows a qualitative difference to the images recorded for the myxobacteria mutants that exhibit typical SPR dynamics [8] as well as to images of SP rods [3-4]. The experiments above also indicate that the bacteria studied here need a liquid surrounding for their flagellar motion and therefore are subject to hydrodynamic interactions in addition to short range steric repulsion encoded in the SPR models. The weakening of the tendency to form clusters has recently been reproduced also by simulations of SPR with hydrodynamic interactions embedded in a fluid [10].

Our results on number fluctuations presented in Supplementary Figure 7 also strongly deviate from the results for different models of self-propelled rods and related experiments with gliding bacteria [8, 11-12], which all exhibited giant number fluctuations (GNF) with an exponent of ~0.8. Here, most experiments, in particular for

the wild-type and short bacteria, show less pronounced GNF with exponent in the range of 0.5-0.6. The large values seen for SP rods without hydrodynamic interaction are approached only for very elongated bacteria (with aspect ratio > 10) at intermediate densities and far away from the transition towards the immotile and jammed phases.

Supplementary References

1. F. Peruani, A. Deutsch, M. Bär, Nonequilibrium clustering of self-propelled rods. *Phys. Rev. E* **74**, 030904 (2006).

2. H. H. Wensink, J. Dunkel, S. Heidenreich, K. Drescher, R. E. Goldstein, H. Löwen and J. M. Yeomans, Meso-scale turbulence in living fluids. *Proc. Nat. Acad. Sci. U.S.A.* **109**, 14308 (2012).

3. M. Abkenar, K. Marx, T. Auth, G. Gompper, Collective behavior of penetrable self-propelled rods in two dimensions. *Phys. Rev. E* **88**, 062314 (2013).

4. S. Weitz, A. Deutsch, F. Peruani, Self-propelled rods exhibit a phase-separated state characterized by the presence of active stresses and the ejection of polar clusters. *Phys. Rev. E* **92**, 012322 (2015).

5. X. Shi and H. Chaté, Self-Propelled Rods: Linking Alignment-Dominated and Repulsion-Dominated Active Matter. *arXiv preprint* arXiv:1807.00294 (2018).

6. R. Großmann, I. S. Aranson, F. Peruani, A particle-field representation unifies paradigms in active matter. *arXiv preprint* arXiv:1906.00277.7 (2019)

8. F. Peruani, J. Starruß, V. Jakovljevic. L. Sogaard-Andersen, A. Deutsch and M. Bär, Collective motion and nonequilibrium cluster formation in colonies of gliding bacteria. *Phys. Rev. Lett.* **108**, 098102 (2012).

9. L. Onsager, The effect of shape on the interaction of colloidal particles. *Ann. New York Acad. Sci.* **51**, 627 (1949).

10. M. Theers, E. Westphal, K. Qi, R. G. Winkler, and G. Gompper, Clustering of microswimmers: interplay of shape and hydrodynamics. *Soft Matter* **14**, 8590 (2018).

11. F. Ginelli, F. Peruani, M. Bär, H. Chaté, Large-scale collective properties of self-propelled rods. *Phys. Rev. Lett.* **104**, 184502 (2010).

12. D. Nishiguchi, K. H. Nagai, H. Chaté, M. Sano. Long-range nematic order and anomalous fluctuations in suspensions of swimming filamentous bacteria. *Phys. Rev. E* **95**, 020601(R) (2017).